Effects of dopants on electronic surface states in InAs

Jonny Dadras,[1,*] Ji Hyun Park,[1] and Christian Ratsch[1,2]
[1]*Department of Mathematics, UCLA, Los Angeles, California 90095, USA*
[2]*Institute of Pure and Applied Mathematics, UCLA, Los Angeles, California 90095, USA*

(Received 19 September 2018; revised manuscript received 25 April 2019; published 11 June 2019)

The effects of several adatom dopants (H, Be, C, N, Si, and Zn) on the electronic structure of low-energy surface reconstructions of InAs—(*001*, *110*, *111*, and *112*) low-index planes—were investigated using *ab initio* density functional theory calculations. It was observed that the local electronic structure can be controlled in such materials, either reducing or enhancing surface states depending on the dopant and the unique surface reconstruction. The local bonding environment, in particular whether the bonding has an aromatic character, was found to influence both surface reconstruction and a dopant's affinity for a surface. Beryllium and Zinc were often found to reduce the surface states around the band gap, which could improve the charge-carrier mobility in various electronic components. However, these dopants can also cause further surface reconstruction/reconfiguration inducing different surface states.

DOI: 10.1103/PhysRevB.99.245406

I. INTRODUCTION

Semiconductor materials are ubiquitous in modern life. In particular, III-V semiconductors have found several applications in pioneering devices, e.g., optoelectronic and nanostructured materials. The physical elucidation of III-V semiconductors is an active area of research. Often such studies look at heterostructures involving several members of these groups, e.g., InAs with GaAs or InSb. The present work focuses on a characteristic example (that of InAs) doped with several experimentally relevant elements. Due to its moderate bandgap of ∼0.36 eV, InAs has applications in infrared detectors, metamaterials, and quantum dots [1–5].

The need to improve device performance, speed, and commercialization typically leads to component miniaturization. This requires strong control over the atomic structure of the material. Experimental limitations over many growth conditions, whether for thin films or nanopatterned materials, often can result in polycrystalline films or multifaceted nanostructures. This can lead to electronic interface or surface states that can hinder the material's performance. Hence, it is essential to understand the nature of such electronic defect states and how these can be passivated or further manipulated to achieve engineering design goals.

The use of a dopant can alter a material's local electronic structure. A doping agent can be used to passivate dangling bonds or enhance or deplete surface charge. In the following, several dopants are studied on low-energy surface reconstructions of the low-index planes of InAs (*001*, *110*, *111*, and *112*). Surface free energies and the electronic structure of the various doped and undoped surfaces are computed using first-principles calculations and compared with each other.

*jonnydadras@outlook.com

II. THEORETICAL METHODOLOGY

Density functional theory (DFT) as implemented in FHI-AIMS [6–8], was employed for structural optimization and electronic-structure calculations. FHI-AIMS is an all-electron program, using atom-centered numerical atomic orbitals; the following calculations used the *Light* basis set, which was found to provide enough accuracy for the present simulations. This basis set goes beyond the minimal basis and includes additional hydrogen-like orbitals, H(nl, z), under a bare Coulomb potential z/r. Similar to the tight-binding approximation, a cut-off potential is employed to eliminate long tails of the radial functions. This takes the form of a screened hard-wall potential to prevent discontinuities in the energy landscape. The basis functions are precomputed and numerically tabulated, leading to O[N] scaling in energy calculations; for further details see Refs. [6,7]. Relativistic corrections were included using the atomic zeroth-order regular approximation. van der Waals corrections were included using the Tkatchenko-Scheffler method [9].

The generalized gradient approximation to the energy functional as given by Perdew, Burke, and Ernzerhof (PBE) [10] was used for energetics and optimizations. However, PBE predicts InAs to be metallic. It has been previously shown that the inclusion of some exact exchange can remedy this deficiency. Consequently, the range-separated hybrid functional given by Heyd, Scuseria, and Ernzerhof (HSE) [11,12] was employed for electronic structure calculations. HSE predicts a bandgap of 0.35 eV, in good agreement with experiment [1]. The choice of functional is motivated by its convenience, accuracy, and that arguments exist for using two different screening parameters for Hartree-Fock and DFT exchange energies [13]. To keep computational costs low, PBE-optimized structures were used for HSE electronic-structure calculations. This only slightly altered electronic properties of interest (e.g., reducing the band gap by ∼20%).

Periodic boundary conditions were enforced for bulk and surface simulations. The eight-atom zincblende bulk unit cell required an $8 \times 8 \times 8$ k-point grid for calculations to reach convergence. For surface-slab simulations a k-point grid of $(8/n) \times (8/n) \times 1$ was used, where n is the number of repeating units in the simulation space. Unwanted dangling bonds were neutralized with pseudohydrogens having partial electrons of 0.75 e (when capping As) or 1.25 e (when capping In). Surfaces were modeled under the repeated slab approach, using appropriate periodic boundary conditions. All slabs were at least five bilayers thick, ensuring minimal interaction between the top and bottom of the slabs. The vacuum gap between repeating slabs was ~20 Å and each lateral dimension was at least ~10 Å, to reduce spurious interactions from repeated images across the periodic boundary.

Surface free energies (γ_S) were computed by

$$\gamma_S = \frac{1}{A}\left(E_{\text{Sys}} - \sum_i \left(\mu_i N_i - \mu_i \frac{N_{H'i}}{C_{\max}} + E_{\text{mol}'i}\frac{N_{H'i}}{C_{\max}}\right)\right). \tag{1}$$

Here A is the lateral surface area, E_{Sys} is the system's DFT energy, i runs over the number of elements, and N_i is the number of atoms of a given element. $N_{H'i}$ is the number of pseudo-H bonding to an element at the bottom layer. $C_{\max}$ is the maximum number of bonds an element can form for In and As $C_{\max} = 4$. $E_{\text{mol}'i}$ is the DFT energy of a pseudo-H-saturated molecule of an element, i.e., XH'_4, with $X =$ In, As, and H' is an appropriate pseudohydrogen. The quantity $N_{H'i}/C_{\max}$ is the fraction of an atom binding to pseudo-H (i.e., the number of dangling bonds being neutralized); these must be subtracted from the total N_i. The sum over i of the last two terms is the surface free energy of the pseudo-H-terminated bottom layer; in the literature this is often called γ_{bottom}. Finally, μ_i is the chemical potential of the i^{th} element. For $\mu_{As(In)}$, the bulk DFT energy per atom of the unit cell was used, a rhombohedral structure for As and tetragonal for In. For dopants, the chemical potential is given by the per atom DFT energies of small elemental gas-phase clusters or molecules, where the dopant would have a similar coordination number as when attaching to a surface.

For simplicity only adatom dopants were studied. Thus, the simulations would represent a concentration density of 10^{18} atoms/m^2 or ~0.1 ML coverage. This may be a limitation of the model, as some dopants may be deposited as, or sinter to, small molecules or clusters. However, the field of single dopant optoelectronics (solotronics) [14–16] is an active area of research where the present simulations could find direct application. Dopant adsorption and substitutional energies (E_{ads} and E_{sub}) were computed from

$$E_{\text{ads}} = E_{\text{Dope}} - E_{\text{Pure}} - \mu_{\text{Elem}} \tag{2a}$$

$$E_{\text{sub}} = E_{\text{Dope}} - E_{\text{Pure}} + \mu_{As(In)} - \mu_{\text{Elem}}, \tag{2b}$$

where E_{Dope} is the DFT energy of the doped surface, E_{Pure} is the energy of the undoped system, μ_{Elem} is the chemical potential of the dopant, and $\mu_{As(In)}$ is the chemical potential of the As(In) being substituted. Hence, negative values are energetically favorable. Given that neither chemical kinetics nor dynamics are modeled, it is stressed that the given values are meant only as a guide to show which dopants have an affinity to attach to a surface.

Lastly, no generally agreed upon definition of a surface-state exists in the community. According to Zangwill [17], the conservation of charge guarantees that $1\,e^-$/atom in the half-filled dangling bond state must be stolen from the bulk states and a deficit in the band charge density corresponds to the creation of a surface-state charge density. Simplifying the problem and to easily visualize changes to the electronic structure, surface states are defined by the deviation of a surface atom's projected density of states (PDOS) away from its bulk PDOS, i.e.,

$$Surf.\,State := \Delta\text{PDOS} = \text{PDOS}[surf.\,atom] - \text{PDOS}[bulk\,atom]. \tag{3}$$

Using this definition, surface sites that are the largest contributors to electronic defect states can be identified and dopant locations can be selected that are more promising. It is noted that integration of these surface states, up to the valence band maximum, would indicate how the partial charge on the atom is altered relative to bulk. Figure 1 presents an example of such surface states for unreconstructed InAs(*001*) (1×1); the top few bilayers were allowed to relax in Z. It is observed that the surface states become negligible below a few bilayers; this was also confirmed for other surfaces. These trends agree with other methods of investigating surface states (e.g., observing the exponential decay of the overlap of the

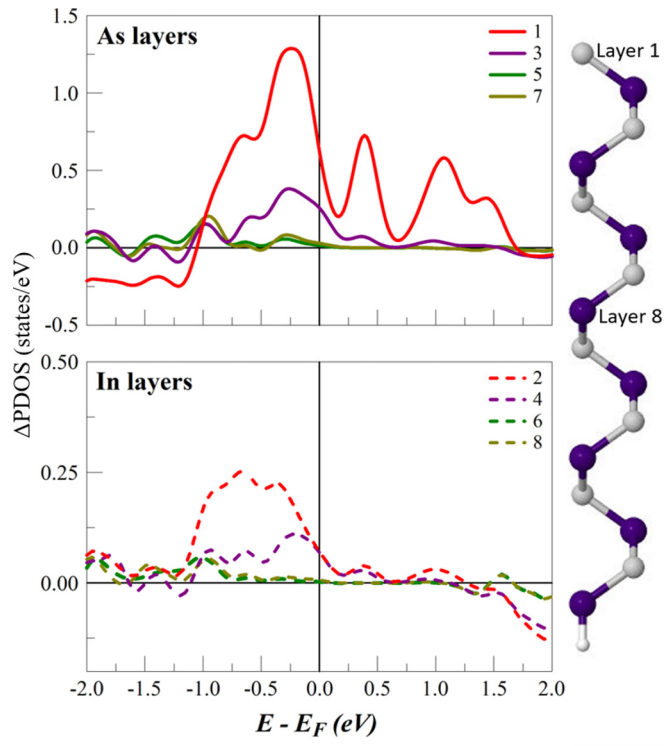

FIG. 1. Surface states of As and In layers in unreconstructed InAs(*001*) (1×1). Odd numbered As layers (top plot, solid lines) and even numbered In layers (bottom plot, dashed lines) are labeled. A side-view schematic shows In atoms in indigo, As atoms as light grey, and pseudo-H is white. It is stressed that the plots are on different scales.

wave function). Additionally, it was observed that indium's surface states were a fraction of those of arsenic's, even when it terminates the top layer. In the next section it will be shown that surface reconstruction aids in reducing, though not eliminating, such electronic defect states.

Alternatively, the band structure in the projected two-dimensional (2D) Brillioun zone can be examined to gain insight about the gross electronic structure of pure and doped surfaces. Figure 2 depicts band structures of a few common low-index surface slabs, the effects resulting from surface reconstruction (or relaxation), and changes arising from a Be dopant; $\boldsymbol{E_F}$ is the Fermi level for a given surface. The first row (A) shows results for unreconstructed surface slabs. It is recognized that these cases are purely academic, as the surface will relax or reconstruct on time scales $\ll 1$ s. However, it is instructive to observe the effects of surface reconstruction on the band structure. The middle row (B) shows the band structures of the different reconstructed and fully optimized surface slabs. The bottom row (C) shows the results when the surfaces are doped. The left column presents results for (*001*) (2×4) surfaces. The middle column shows the bands for the (*110*) planes. The column on the right depicts the bands for the (*111*)A cleavage. Therefore, the particular surface reconstructions examined are pure and doped InAs(*001*) $\alpha_2(2 \times 4)$, InAs(*110*) (2×2), and InAs(*111*)A (2×2) In vacancy. The selected path corresponds to moving in the k space of the 1×1 unit surface, i.e., letting $k_Z = 0$, the path is $(0.5, 0.0) \rightarrow (0.0, 0.0) \rightarrow (0.5, 0.5) \rightarrow (0.0, 0.5)$, while taking into account the appropriate number of *mxn* foldings from each repeating unit of a given surface.

Certainly, important information can be gained from this analysis. For example, Be substituting a top-layer In atom changes the InAs(*110*) surface from a semiconductor to a semimetal. Additionally, when the In vacancy in InAs(*111*)A (2×2) is doped with Be, the surface changes from a direct, to an indirect and narrow band gap semiconductor. It is noted that the band structure of InAs(*001*) $\beta_2(2 \times 4)$ (not shown) behaves qualitatively similar to that of InAs(*001*) $\alpha_2(2 \times 4)$. However, the former is a direct bandgap semiconductor, while the latter is observed to be indirect. The Be dopant adsorbing on either surface reconstruction's trench dimer only mildly alters their band structures. The case of InAs(*111*)B (2×2) will be discussed later. However, for the present purposes, there are several issues that arise by only studying band structure plots. One such issue is that reconstructed surfaces can be more complex than bulk crystals. This makes the search for a unique path through k space, which captures all the high-symmetry points, especially challenging. Additionally, a more detailed microscopic understanding is gained by studying surface states as defined above, e.g., determining which atoms are the biggest contributors to surface states. Such theoretical predictions become more relevant to experiment as the need for atomic level control increases with technological advancement and miniaturization.

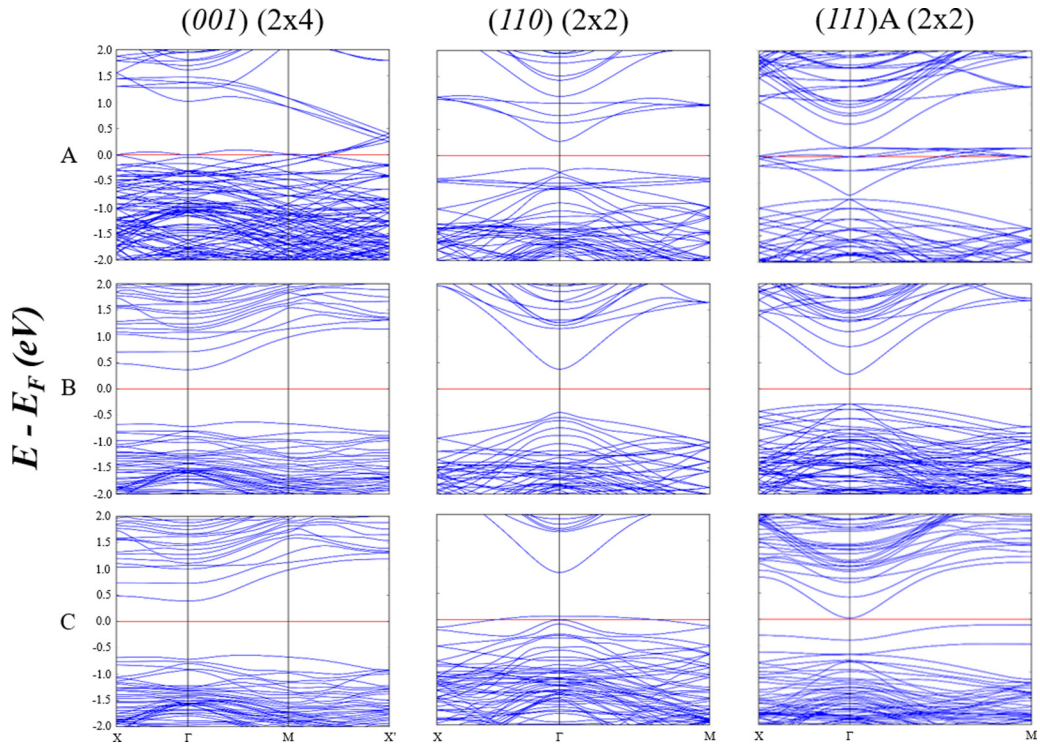

FIG. 2. Band structure plots of several surface slabs. The column on the left, shows data for (*001*) (2×4) slabs. The middle column displays band plots for (*110*) (2×2) slabs. The column on the right, shows results for (*111*)A (2×2) slabs. Row A is an academic scenario of a cleaved unoptimized surface. Row B shows data for fully relaxed/reconstructed surfaces of InAs(*001*) $\alpha_2(2 \times 4)$, InAs(*110*), and InAs(*111*)A (2×2) In vacancy. Row C shows results of the same surfaces doped with Be: Adsorbing on the trench dimer (left), substituting a top layer In atom (middle), and adsorbing on top the In vacancy (right).

III. RESULTS

A. Undoped low-index planes of InAs

Experimental growth conditions are complex and can allow for the formation of several surface facets. To model these diverse scenarios, several low-index planes were selected (*001*, *110*, *111*, and *112*), as these are experimentally more relevant and energetically preferred. Each cleavage can have its own energetically favorable reconstructions. Previously, one of the authors (Ratsch) as well as several other groups have made detailed studies of such surface reconstructions [18–23]. The selected surfaces-reconstructions were those previously found to be the most energetically favored across the majority of the As chemical potential range. Figure 3 shows a phase diagram of the lowest energy surfaces across the range of As-poor ($\Delta\mu_{As} = \mu_{InAs}{}^{(b)} - \mu_{In}{}^{(b)} - \mu_{As}{}^{(b)} = -0.53\,\text{eV}$) and As-rich ($\Delta\mu_{As} = 0$) conditions. It is noted that InAs(*110*) does not reconstruct, in the sense that the lateral symmetry of the surface is preserved after relaxation. However, the top layer In atoms relax into the surface while the top As atoms slightly extend outward from their bulk positions. Some authors call this surface-reconfiguration [24]. For further details on the reconstructions of (*001*), (*111*), and (*112*), see Refs. [18–23], and references therein.[1]

Figure 4 shows a schematic of the six relaxed surfaces investigated. A clean cut along the (*001*) direction results in the creation of two dangling bonds per surface atom. To minimize this effect, the interface atoms can dimerize, resulting in only one dangling bond per atom. There are two well-known stable surface reconstructions across most of the As chemical potential range, known as InAs(*001*) $\alpha_2(2\times4)$ and $\beta_2(2\times4)$. Cleaving InAs along the (*110*) direction results in only one dangling bond per atom. To further minimize the energy, the In atoms take on a deformed sp^2-hybrid bonding character; the top layer In atom relaxes into the slab and the As atom is slightly displaced out. This aromatic

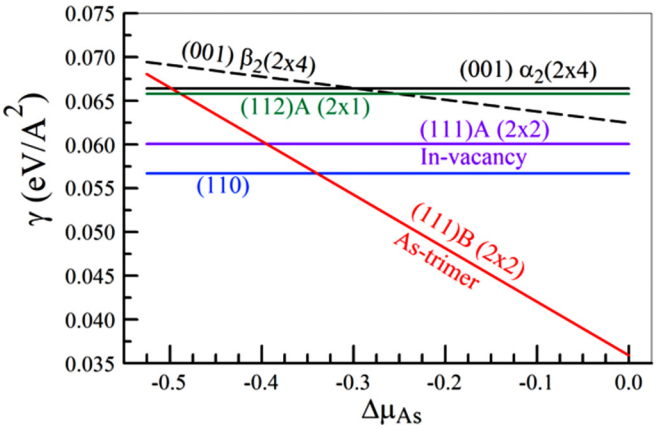

FIG. 3. Phase diagram of the lowest energy reconstruction for (*001*) in black, (*110*) in blue, (*111*)A in purple, (*111*)B in red, and (*112*)A in green. The (*001*) cleavage has two favorable reconstructions that dominate over the chemical potential range, $\alpha_2(2\times4)$ (solid line) and $\beta_2(2\times4)$ (dashed line). For simplicity, the well-studied (*001*) $c(4\times4)$, (*111*)A (2×2) As trimer, and (*111*)B (2×2) As-vacancy reconstructions were not included in the present work.

[1]This is not an exhaustive list of surface reconstructions for the listed low-index planes. Namely the (*001*) $c(4\times4)$, (*111*)A As trimer, (*111*)B As-vacancy reconstructions, and the (*112*)B surface are not included. This was motivated by the need to be concise and the fact that those surface reconstructions were favored only for a small fraction of chemical potential space.

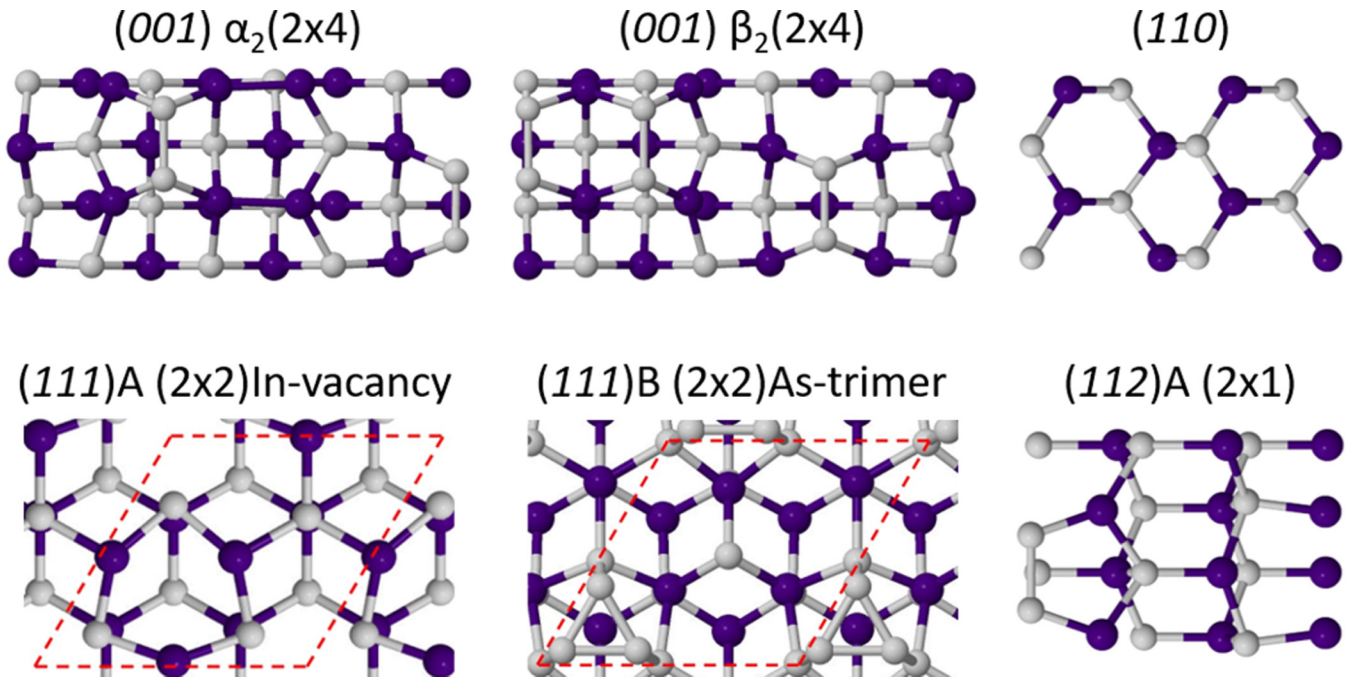

FIG. 4. Top view schematics of the six low-energy surface reconstructions/reconfigurations studied: InAs(*001*) $\alpha_2(2\times4)$ and $\beta_2(2\times4)$, InAs(*110*), InAs(*111*)A In vacancy (note the In vacancy is at the corner of the 2×2 unit cell), InAs(*111*)B As trimer, and InAs(*112*)A.

character aids in minimizing the creation of surface states near $\boldsymbol{E_F}$, as shown in the following. The InAs(*111*) cleavage has two stoichiometric configurations, an In-terminated case (A-type) and an As-terminated case (B-type). Each of these can have several potential reconstructions. Only the lowest energy 2×2 surface reconstruction, which spans most of $\Delta\mu_{As}$, was investigated for each cleavage. These are the InAs(*111*)A In vacancy and the InAs(*111*)B As trimer. Unlike the case of (*001*), A and B surface types are strictly determined by the substrate. Removing half a bilayer would result in the formation of three dangling bonds per atom, which is energetically forbidden. For the (*111*)A In-vacancy reconstruction, the As atoms surrounding the vacancy all bind to In atoms taking the perturbed sp^2 configuration, i.e., the surface interface is nearly atomically flat. The As atoms forming the trimer in the (*111*)B As-trimer reconstruction each have one dangling bond and are in a ring structure, indicating a likely aromatic character to the bonding. The As atom in the canyon between the trimers will have one dangling bond. The InAs(*112*) facet also has A and B stoichiometric surfaces. For simplicity, only the InAs(*112*)A (2×1) reconstruction was examined; the top pair of As atoms dimerize and the In atoms relax into the surface, again acquiring a distorted sp^2 bonding character.

Bonding on surfaces is complex and cannot be fully explained by simple molecular symmetry arguments. Indeed, a complete molecular orbital bonding analysis is beyond the scope of this work. However, some simple heuristics can be given to further justify the claims regarding the aromatic nature of the bonding. For the dimerized systems, i.e., InAs(*001*) $\alpha_2(2 \times 4)$ and $\beta_2(2 \times 4)$ and InAs(*112*)A (2×1), the As-In-As angle pointing out away from the structure on which the dimer sits, going toward the top or bottom of Fig. 4, is typically about 140°; the other two angles are approximately 110°. For the InAs(*111*)A In-vacancy surface reconstruction, the larger As-In-As angle is also of about 140°, pointing toward the center of the six-membered ring structure shown in Fig. 4. Again, the other two remaining angles are about 110°. For InAs(*110*), the angle pointing out of the plane, away from the slab, is about 110° and the two angles directed into the slab are each about 125°. To give estimates of the degree of planarity of the mentioned $InAs_3$ subunits on the surfaces, a measure of the dihedral angles (φ) can be used. The dihedral angles for InAs(*001*) $\alpha_2(2 \times 4)$ and $\beta_2(2 \times 4)$ reconstructions are $\varphi = 6.7^\circ$ and 9.1°, respectively, demonstrating that the four-atom subunit is more planar on the $\alpha_2(2 \times 4)$ reconstruction. The $InAs_3$ subunit of InAs(*110*) has $\varphi = 10.8^\circ$. On the InAs(*111*)A In-vacancy reconstruction the subunit has $\varphi = 4.7^\circ$, while for InAs(*112*)A (2×1), $\varphi = 6.3^\circ$.

Surface reconstruction aids in reducing the prominent surface states like those shown in Fig. 1. For an example, a selected atom's surface states from the two undoped InAs(*001*) surface reconstructions are presented in Fig. 5. In both cases, it is observed that As atoms in the trench dimers, which are off-axis from the top dimers, have more pronounced surface states. However, the $\beta_2(2 \times 4)$ top dimers do have a pronounced signature. The reason for this can be found by inspecting the inset structures shown in Fig. 5 and the previous statements. For $\alpha_2(2 \times 4)$ the In atoms below the top dimer, nearest the trench dimer across the periodic boundary (shown on the left), is allowed to better adapt to a warped sp^2-hybrid

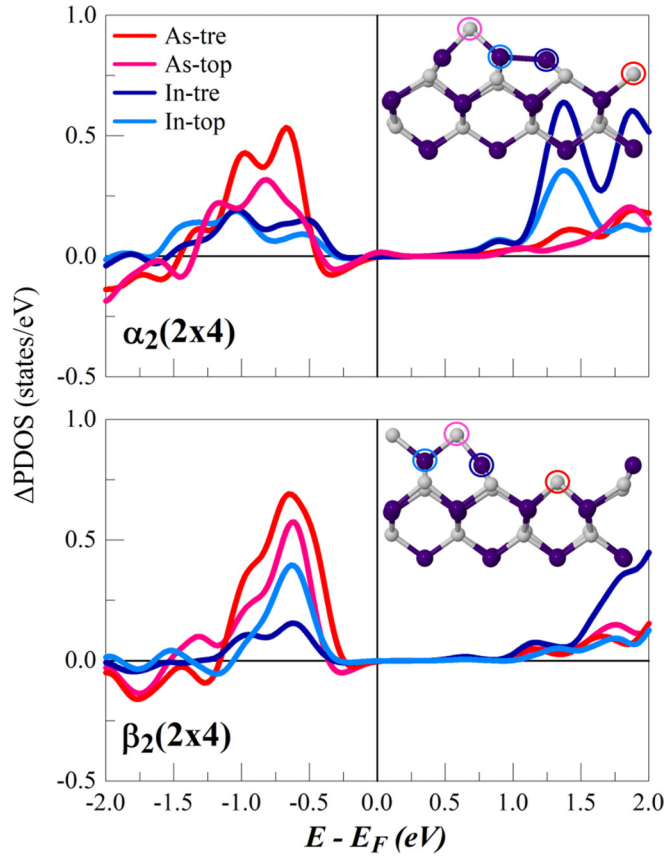

FIG. 5. Surface states of the InAs(*001*) $\alpha_2(2 \times 4)$ and $\beta_2(2 \times 4)$ surface reconstructions. Inset schematics show circles around selected atoms that are colored to correspond with the plots. In both cases, As atoms in the trench dimers are the biggest contributors to electronic surface states.

configuration. This aids in the reduction of the surface states arising from the top dimer. Due to the symmetry of the pair of top dimers in $\beta_2(2 \times 4)$, this reconfiguration is strained and therefore the As atoms forming the top dimers still have notable perturbed densities. As shown in Fig. 1, indium's surface states near $\boldsymbol{E_F}$ are all relatively small and this was observed for the other surfaces.

B. Doped low-index planes of InAs

Given that it is often a goal to control surface states, typically reduce them, only the atoms with the most pronounced surface states are studied for the remainder of this work. It was observed that the preferred binding sites for most of the dopants were near an As atom with the most prominent surface states. In the few instances where another site was preferred, the energy differences were on the order of a few tens of meV. Although the individual contributions of all the atoms for the various surface orientations and reconstructions were examined, only the results of doping near an As atom that is the largest donor to surface states are presented. Hence, half a dozen experimentally relevant dopants—H, Be, C, N, Si, and Zn [25]—were adsorbed or substituted on to a surface near a selected As atom. The ΔPDOS of the given As atom was then computed for the doped case and compared with the ΔPDOS of the undoped (i.e., pure) case.

TABLE I. Dopant substitutional and adsorption energies on InAs(*001*) $\alpha_2(2 \times 4)$ and $\beta_2(2 \times 4)$ surface reconstructions. Be and Zn show a good affinity for the surfaces to adsorb or substitute. Si is only slightly disfavored to substitute, but does show a preference to adsorb.

	InAs(*001*) $\alpha_2(2 \times 4)$		InAs(*001*) $\beta_2(2 \times 4)$	
Dopant	E_{sub}(eV)	E_{ads}(eV)	E_{sub}(eV)	E_{ads}(eV)
H	0.65	0.69	0.51	0.67
Be	**−0.99**	**−2.54**	**−1.00**	**−2.55**
C	2.39	1.77	2.39	1.86
N	0.58	0.65	0.50	0.66
Si	0.17	**−0.24**	0.24	**−0.46**
Zn	**−0.37**	**−1.61**	**−0.37**	**−1.62**

Inset schematics of the surfaces, shown the figures below, represent the initial configurations of the doped system. In general, the final state configuration was similar to the initial state. For the unique case of H, the initial position of the doped system was perturbed such that the H would bind with the selected As atom. Again, given the uncertainty in obtaining the chemical potential of a given element, presented adsorption and substitutional energies show whether a certain dopant has an affinity for a surface and does not represent an absolute binding energy.

1. InAs(001) surfaces

In Table I, the adsorption and substitutional energies of the various dopants on the InAs(*001*) surface reconstructions are presented. Be and Zn are found to have good affinities to attach with either surface reconstruction as either is an adsorbent or substituent. Si shows good affinity as an adsorbent on the trench dimers.

Figure 6 shows the surface states of the pure and doped surface reconstructions. The inset structural schematics show the initial configuration of the dopant adsorbing or substituting one of the As atoms in the trench -dimer. Be and Zn both drive the main peak of the surface state down deeper in the valence band, away from $\boldsymbol{E_F}$, while not introducing any pronounced unoccupied states in the conduction band. Also, Be and Zn (as substituents) have a similar effect on the surface states. Hydrogen, as a substituent, does well to push the density into the valence band, but, it must overcome a ∼0.5-eV barrier to substitute the As atom.

2. InAs(110) surface

Table II presents the substitutional and adsorption energies of selected dopants on the InAs(*110*) surface. Again, for simplicity only the effect on As's surface states when substituting an In atom is presented. Be, Zn, and Si all show an affinity for attaching to the surface in either an adsorbing or substituting arrangement.

Figure 7 presents the surface states for the pure and doped InAs(*110*) surface. The preferred initial adsorption site and the In-substitutional case are shown in the inset of Fig. 7. For the case of adsorption, Be, Si, and Zn push the surface states up toward $\boldsymbol{E_F}$ and show increased amplitudes. However, as substituents, these dopants introduce states in the band gap. Only H acting as a substituent shows noted reduction in the density within the valence band, although some unoccupied states arise about 1 eV above $\boldsymbol{E_F}$ and there is a relatively large energy barrier of 1 eV to overcome.

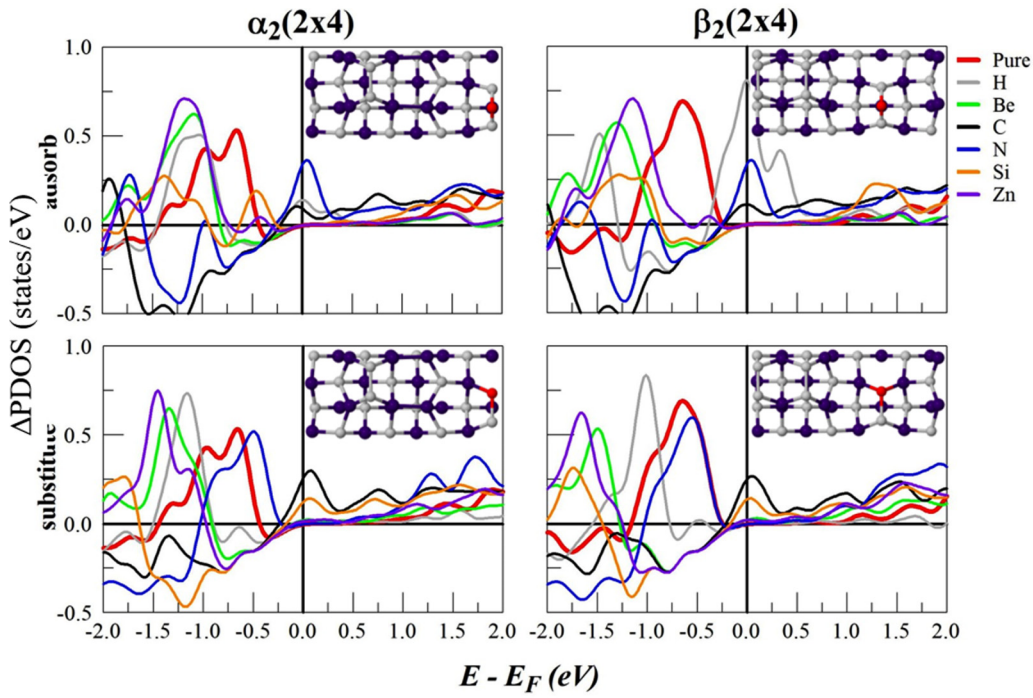

FIG. 6. The effect of dopants on surface states of a selected As atom in the trench dimers in InAs(*001*) $\alpha_2(2 \times 4)$ and $\beta_2(2 \times 4)$ reconstructions. Be and Zn consistently draw the electron density away from the Fermi level deeper into the valence band.

TABLE II. Dopant substitutional and adsorption energies on InAs(*110*). Be, Si, and Zn show good affinity to adsorb or substitute on this surface.

	InAs(*110*)	
Dopant	E_{sub}(eV)	E_{ads}(eV)
H	1.00	0.55
Be	**−1.48**	**−1.34**
C	2.27	2.35
N	1.57	1.10
Si	**−0.11**	**−0.27**
Zn	**−0.51**	**−0.87**

3. InAs(111)A surface

For the InAs(*111*)A (2 × 2) In-vacancy reconstruction, the preferred binding site of the dopant was (in general) atop the vacancy site. Table III lists the adsorption energies for the dopants to attach near the vacancy. Be, Zn, and Si again show an affinity to stick to this surface reconstruction.

In Fig. 8, changes to the PDOS of an As atom near the In vacancy of this surface reconstruction are shown. The undoped (*111*)A In-vacancy reconstruction already presents small surface states; Be, Zn, and Si alter these. Hydrogenation shows slight reduction to parts of the PDOS, relative to the pure surface. However, overall the amplitudes are comparable to the undoped surface and nearly all the dopants introduce conduction band states.

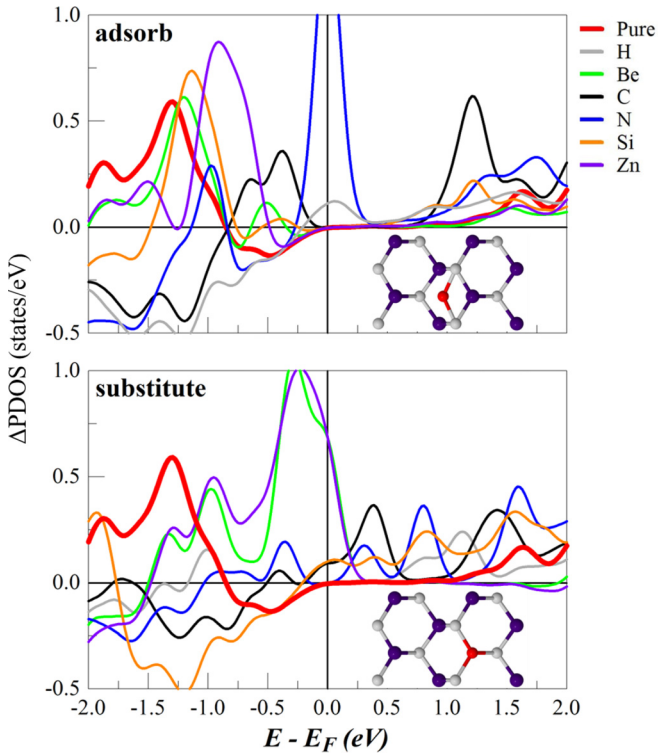

FIG. 7. Effect of dopants on surface states of a top layer As atom in InAs(*110*). For the case of adsorption; Be, Zn, and Si mildly shift the surface states up toward E_F. Substitution of the In atom generally increases the As surface state, except for the case of H.

TABLE III. Adsorption energies for dopants on the InAs(*111*)A (2 × 2) In-vacancy reconstruction. Be, Si, and Zn have a good affinity to adsorb on top of the vacancy.

Dopant	InAs(*111*)A In vacancy E_{ads}(eV)
H	0.25
Be	**−2.13**
C	2.58
N	1.57
Si	**−0.18**
Zn	**−0.91**

4. InAs(111)B surface

Table IV lists the adsorption energies for dopants on the InAs(*111*)B (2 × 2) As-trimer reconstruction. Dopants are attached on top of the As atom that is in the canyon between As trimers, see Fig. 4. This atom showed pronounced surface states, whereas those for the As atoms forming the trimer were small. Substitution of any As atom was energetically prohibited for all dopants. Both Be and Zn show an affinity to adsorb on this site.

Figure 9 presents the surface states of the doped and pure (*111*)B As-trimer reconstruction. However, this reconstruction is more involved and the dopants can significantly alter the final state configuration (discussed below). To avoid misleading the reader, no inset of the initial configuration is shown. A pronounced peak is observed for the As atom flanked by the trimers. Here, Be and Si greatly reduce the number of surface states and Be nearly eliminates them. Doping with Zn also nearly removes the surface states, except for a narrow peak at around ∼0.75 eV below E_F.

5. InAs(112)A surface

For the InAs(*112*)A (2 × 1) reconstruction dopants were adsorbed in a bridging position with the top As dimer or substituting one of the As atoms in the dimer. Table V lists the substitutional and adsorption energies for the dopants on this

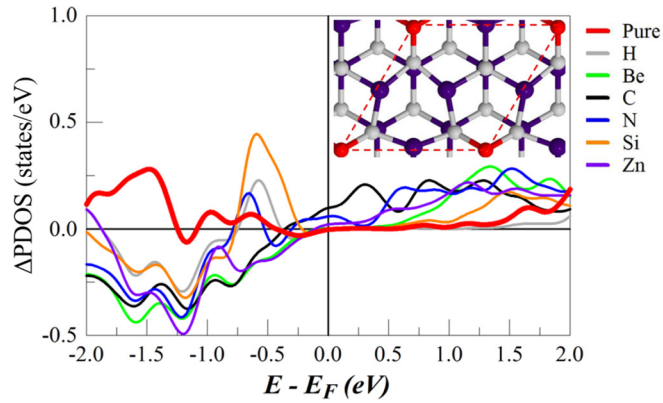

FIG. 8. Surface states of the pure and doped InAs(*111*)A (2 × 2) In vacancy. Only H leads to minimal alteration of the already small surface states of the As atoms around the vacancy.

TABLE IV. Dopant adsorption energies on the InAs(*111*)B (2 × 2) As-trimer reconstruction. Be and Zn show an affinity to adsorb atop the selected As atom.

Dopant	InAs(*111*)B As trimer E_{ads}(eV)
H	0.18
Be	**−1.59**
C	2.80
N	2.40
Si	0.43
Zn	**−0.98**

TABLE V. Substitutional and adsorption energies of dopants on the InAs(*112*)A (2 × 1) surface reconstruction. Be and Zn again show good affinity to attach on this surface.

	InAs(*112*)A	
Dopant	E_{sub}(eV)	E_{ads}(eV)
H	0.34	0.74
Be	**−1.00**	**−2.42**
C	2.49	1.90
N	0.38	0.73
Si	0.32	0.14
Zn	**−0.30**	**−1.46**

surface reconstruction. Again, Be and Zn show good affinity for the surface, while the other dopants must overcome energy barriers.

In Fig. 10, the surface states are shown for the doped and undoped InAs(*112*)A (2 × 1) reconstruction. Similar to trench dimers in the InAs(*001*) $\alpha_2(2\times4)$ and $\beta_2(2\times4)$ reconstructions, it was observed that Be and Zn push the main peak deeper into the valence band. Additionally, doping with Be or Zn did not tremendously alter surface-state amplitudes, typically mildly increasing them. It is noted, that as substituents, Be and Zn lead to small peaks in the density at $\boldsymbol{E_F}$. This could be an artefact of theory as the amplitudes are below the level of 0.1.

IV. DISCUSSION

A. Undoped surfaces

The above results demonstrate that adatom dopants generally alter the surface states created beyond surface relaxation or reconstruction. Surface reconstruction or reconfiguration leads to a characteristic change in the PDOS of a surface As atom, relative to an As atom in bulk InAs, as observed across all studied low-index planes. Going down into the valence band from the Fermi level, the surface states first dip down, indicating a reduction of electron density relative to an As atom in bulk InAs. Within the valence band, around 1 eV below $\boldsymbol{E_F}$, a positive peak on the order of ∼0.5 is created, indicating an increase in electron density relative to the atom in bulk. Typically, the amplitudes of the surface states then decrease as one moves deeper into the valence band. It is also commonly observed that a slight population of conduction band states are created around 1.5–2.0 eV above $\boldsymbol{E_F}$.

Overall, the undoped surface with the smallest surface states is the InAs(*111*)A-In vacancy. It is argued that this is a result of the As atoms bonding with In atoms that are in a contorted sp^2-binding configuration. This was a general trait of several surfaces, which the introduction of aromatic bonding reduced the surface states, either showing peaks at

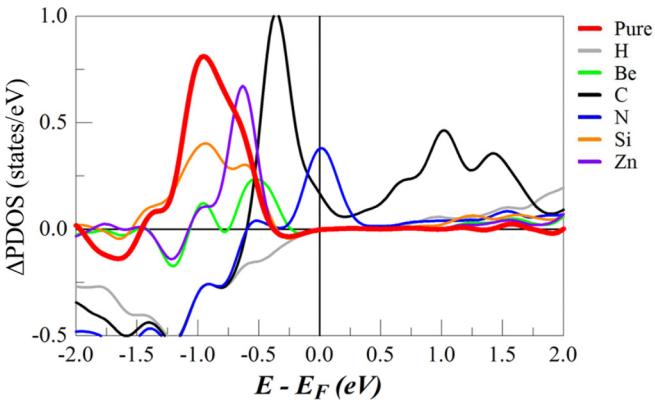

FIG. 9. Surface states of the doped and pure the InAs(*111*)B (2 × 2) As-trimer reconstruction. Be, Zn, and Si lead to a noted reduction of the surface-state amplitudes; Be nearly eradicates them.

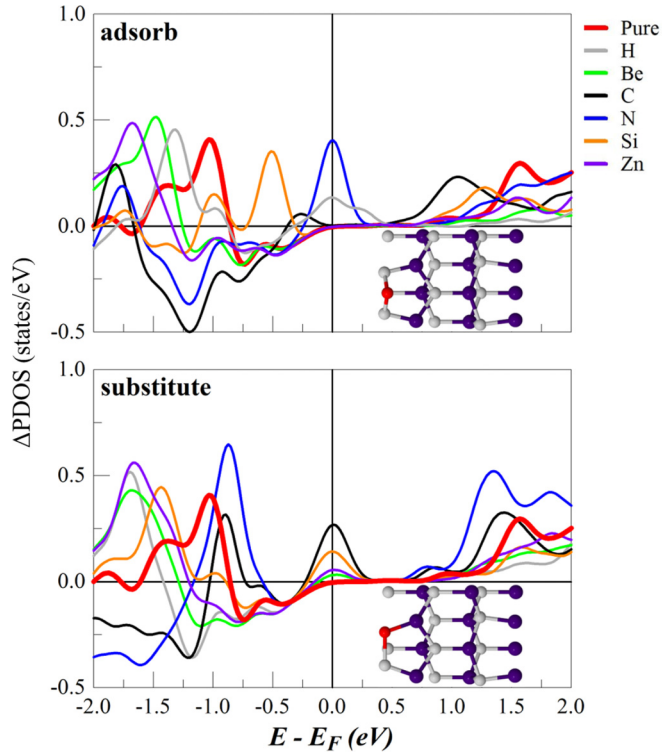

FIG. 10. Surface states for adsorbing and substituting dopants in the top layer As dimer in the InAs(*112*)A (2 × 1) reconstruction. For the case of adsorption, Be and Zn drive the main peak down into the valence band. However, as substituents these elements lead to very small peaks at $\boldsymbol{E_F}$.

or below ∼1 eV from $\boldsymbol{E_F}$. Aromatization, which eliminates dangling bonds and thus surface states, is a driving force in surface reconstruction and relaxation. This is not too surprising, as Zangwill [17] points this out for elemental group-IV semiconductors.

B. Effects of biologic dopants (H C N)

The biologic dopants increase the electron density around the Fermi level. Hydrogenation sometimes quenches the peak remaining after surface reconstruction. But often a population is created at $\boldsymbol{E_F}$, or a population inversion occurs, where the density in the valence band becomes negative and the conduction bands become more populated. Regardless, there is an energy barrier to attach H to any low-index surface of InAs that ranges from ∼0.25−1.0 eV. Coking, i.e., depositing C, always creates electronic states at or near $\boldsymbol{E_F}$. Simultaneously, C will often invert the main peak of the undoped surface, thus inverting the population density relative to bulk. For the surfaces studied, the attachment of C must overcome energy barriers in the range of ∼1.5−2.5 eV. Nitrogenation of InAs has the effect of at least narrowing the gap between valence and conduction band states. However, more often N doping leads to the creation of a pronounced peak at the Fermi level and can also partially invert the main peak of the clean surfaces. Attaching N to the InAs surfaces requires overcoming energy barriers ranging from ∼0.5 to 2.5 eV.

The introduction of H, C, or N dopants induce the formation of gap states for surface As atoms. This alters the conductive properties and implies that the surfaces have become (semi)metallic. Additionally, attaching any of H, C, or N demands surpassing an energy barrier on the order of 1 eV, indicating that experiments would typically need to be done at higher temperatures and/or using beam methods that could damage, or otherwise alter the surface and the bulk material. This could lead to further electronic surface and defect states.

C. Effects of the Group IIA, IIB, IVA dopants (Be Zn Si)

As noted in the previous section, doping InAs with other non-III-V metals and metalloids can drive the main peak of the surface states down into the valence band or greatly reduce their amplitudes. These elements more readily attach to the surface compared with the biologic elements. Silication of the surfaces generally does increase the density in the conduction band. Si-doping, as a substituent, leads to the development of gap states and can lead to the inversion of the main peak from the clean surface. When adsorbing on a surface, Si often draws the main peak density out of the valence band toward $\boldsymbol{E_F}$. However, adsorption on InAs(*001*) $\alpha_2(2\times4)$ and $\beta_2(2\times4)$ and the InAs(*111*)B (2×2) As-trimer reconstructions noticeably reduces the surface states compared with the pure surfaces. Silicon will typically bind as an adsorbent, with E_{ads} in the range of about −0.5−0.1 eV, while substitutional energy barriers are of the same magnitude. Doping with either Be or Zn shows similar trends. This result is not too surprising as Zn is chemically similar to Mg (immediately below Be), having a normal oxidation state of +2 [26]. Hence, Be and Zn will have similar chemical reactivities and also lead to similar mechanical distortions in the crystal structure. When the undoped system already has surface states that are small or are deeper in the valence band, Be and Zn will not reduce these and can introduce gap states and/or invert populations depending on the nature of the bonding. On the other hand, when a clean surface has more pronounced defect states closer to $\boldsymbol{E_F}$, Be and Zn drive the main peaks deeper into the valence band or can greatly reduce the amplitudes. This effect is especially notable for these dopants adsorbing on InAs(*001*) $\alpha_2(2\times4)$ and $\beta_2(2\times4)$, InAs(*111*)B (2×2) As trimer, and the InAs(*112*)A (2×1) surface reconstructions. Lastly, Be and Zn almost always show good affinity for attaching to the low-index surfaces of InAs, with Be typically having an attachment energy two or three times that of Zn.

To elucidate the origins of the changes in some of the surface states, the nature of the bonding on the surface is examined in more detail. Figure 11 shows schematics of optimized structures for Zn substituting in InAs(*001*) $\alpha_2(2\times4)$, Be adsorbing on InAs(*001*) $\beta_2(2\times4)$ and InAs(*112*)A (2×1), and Zn adsorbing on the InAs(*111*)B (2×2) As trimer. The structural changes and nature of the bonding for both Be and Zn is quite similar and only the mentioned examples are discussed. When adsorbing on As dimers, it is found that these dopants push the As atoms toward their unreconstructed positions, binding in a linear configuration. Moreover, as when the As atoms were dimerized, doped As atoms will have one dangling bond. This is the reason for the surface states being pressed into the valence band, though not being reduced in amplitude. It is noted that adding an additional adatom dopant, outside of and coaxial with the dimer, should quench the remaining dangling bond and thus greatly reduce the number of surface states around the bulk band gap. When Be or Zn are substituted into a dimer, the remaining As also moves towards its unreconstructed position and the dopant takes on a broken sp^2 symmetry, resulting in similar surface states as in the case of adsorption.

The unique case of a dopant on the (*111*)B As-trimer reconstruction, results in the dopant acquiring an aromatic character. But, this is at the expense of the As trimer opening and forming zig-zag chains of $As_3Y (Y = \text{Be, Zn})$ stoichiometries. The resulting (sp^2-like) YAs_3 subunits have As-*Y*-As angles pointing away from the slab that are 122° and 128° for Be and Zn doping, respectively. Consequently, the two angles pointing towards the slab are 117° for Be and 112° for Zn. The dihedral angles for Be and Zn doping are found to be $\varphi = 12.4^\circ$ and 16.3°, respectively. Hence, the Be-doped subunit is more planar than the Zn-doped one. Figure 12 shows the resulting surface states for the As atoms that formerly composed the trimer, compared with those of the undoped As-trimer atoms. The two first nearest neighbor (NN) atoms to the dopant show large peaks in their surface states at about ∼0.5 eV below $\boldsymbol{E_F}$. The remaining second NN As atom (that is not covalently binding) to the dopant, has much smaller amplitude states. Though these are still more pronounced than the states of the undoped As trimer. The addition of a second dopant, near the initial center of the trimer, may aid in eliminating these induced surface states.

For thoroughness, the band structures of pure and Be- and Zn-doped InAs(*111*)B (2×2) As trimer are shown in Fig. 13. The path through k space was defined as in Fig. 2. It is

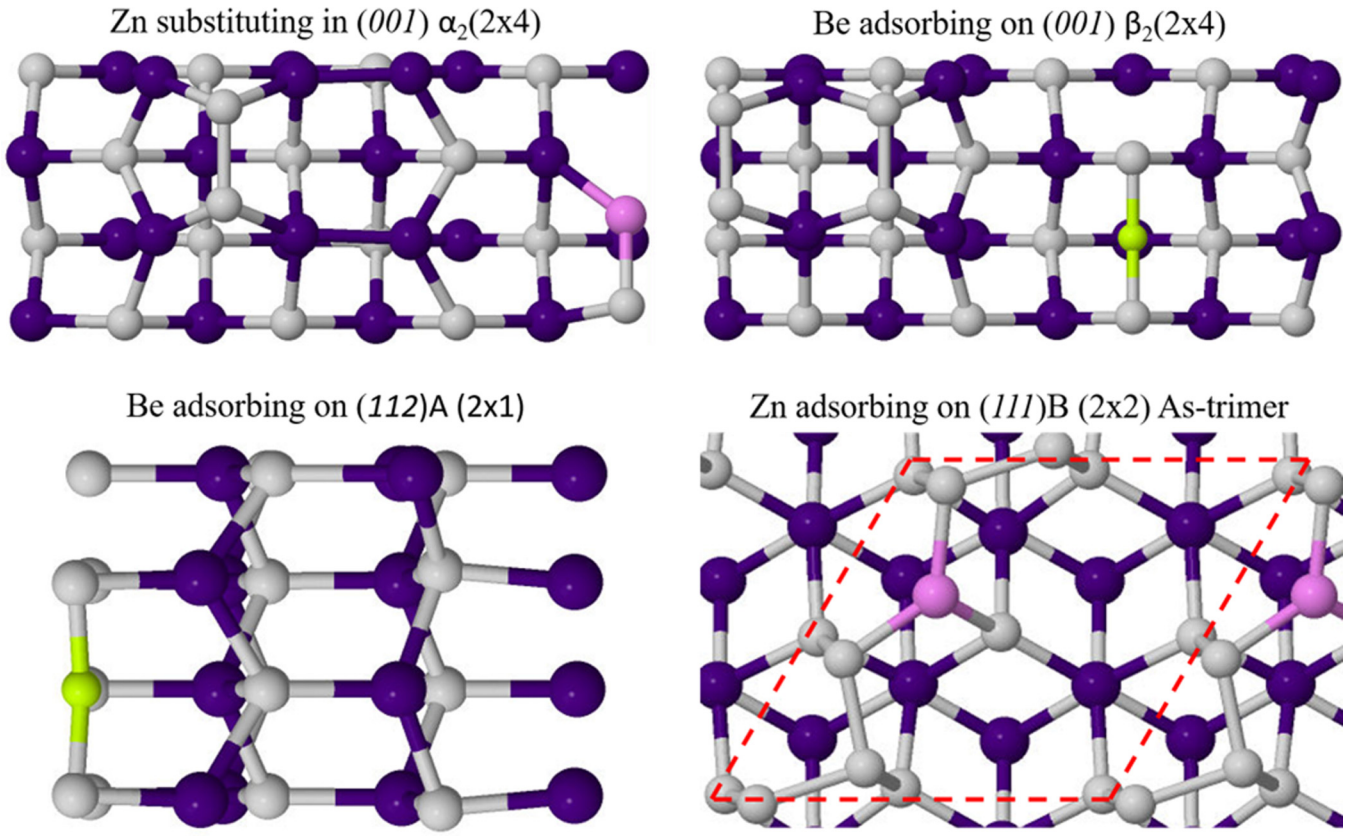

FIG. 11. Schematics of optimized surfaces doped with Be or Zn. The dopants act to return As-dimer atoms to their bulk unreconstructed positions, aiding in surface states being drawn away from the Fermi level. When adsorbing on the (*111*)B As-trimer reconstruction, the dopants acquire an sp^2 quality at the expense of unfastening the trimer to form chains.

observed that the undoped surface (*a*) is a direct band gap semiconductor. When doping with Be (*b*), the surface remains a direct back gap semiconductor, i.e., the difference between the smallest direct and indirect gaps is below the level of 1 meV, while Zn doping (*c*) leads to an indirect band gap that is about 40-meV smaller than any direct band gap. This can be observed in the band structures, where the indirect character of the Zn-doped surface is more pronounced.

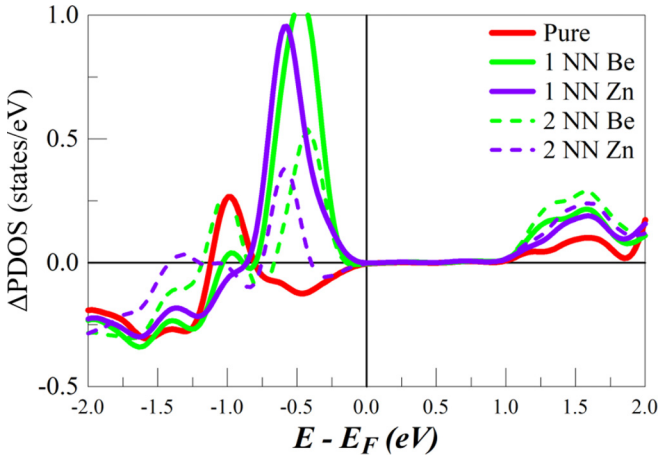

FIG. 12. Surface states of As atoms forming the trimer on the InAs(*111*)B (2 × 2) As-trimer reconstruction. The undoped system has very small surface states. Be and Zn create fairly narrow, pronounced surface states for the As atoms that are first NNs. The second NN atom that does not directly bind with the dopant, shows less prominent peaks. However, these surface states are more marked than the states of the pure As trimer.

D. Comparison with other investigations of doped III-V materials

It is interesting to compare with theoretical investigations that studied one of the current dopants on another common III-V material. One such study, carried out by Miotto *et al.*, examined GaAs(*001*) $\beta_2(2 \times 4)$ with a Zn dopant adsorbing at different locations on the surface [27]. They observed that the preferred binding site was on the trench dimer, in qualitative agreement with the present findings. Additionally, they found that there is also a restructuring leading to a slightly buckled (∼0.1 Å out of the plane) linear As-Zn-As trimer. From their results, it is unclear whether the surface has a direct or indirect band gap. However, they show that the presence of Zn only mildly alters the band structure (in agreement with the results discussed in Sec. II). For further details see Ref. [27].

The impacts of some of the studied dopants has been investigated experimentally, often in terms of the mechanical effects. For example, Castleton *et al.* [28]. showed that H^+ adsorption on InAs(*110*) would lead to charge accumulation that could result in scanning tunneling microscopy (STM) images similar to those for an As vacancy in that system.

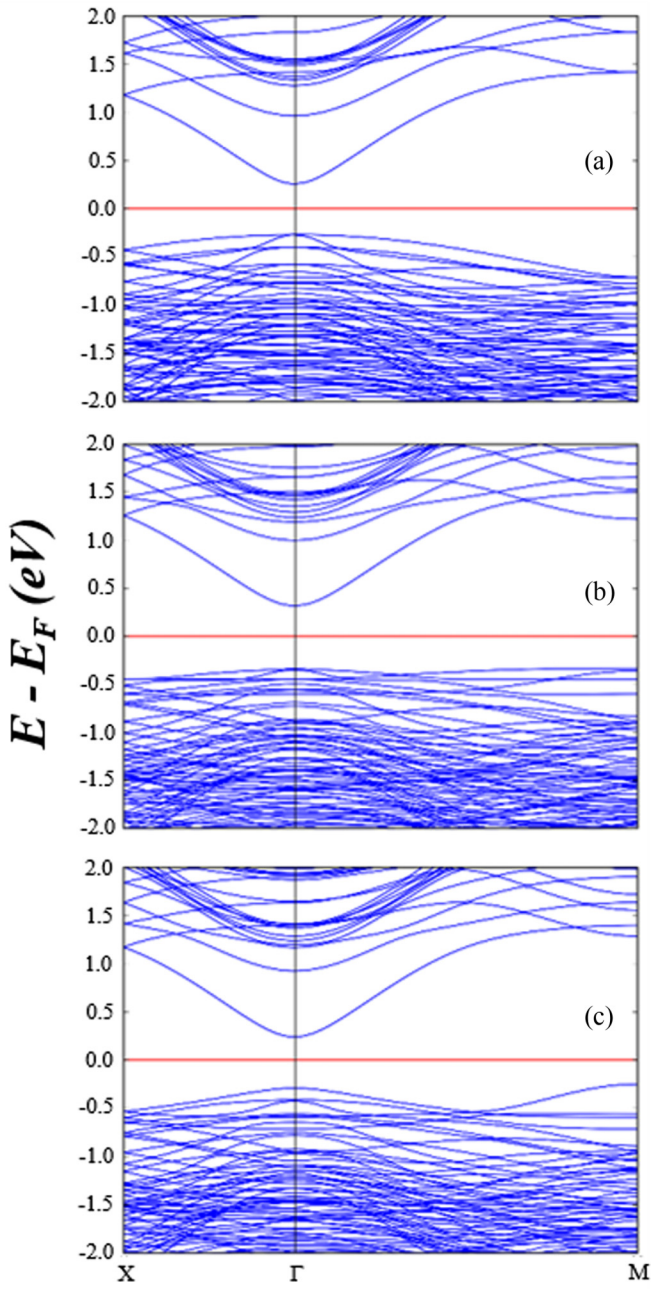

FIG. 13. Band structure plots of the InAs(*111*)B (2 × 2) As trimer; pure (*a*), Be-doped (*b*), and Zn-doped (*c*). The pure and Be-doped surfaces have a direct band gap, while doping with Zn makes the surface an indirect band gap semiconductor.

Ghoneim *et al.* [29] studied axial (*111*), radial (*110*) InAs nanowires and found that doping with C will drastically reduce nucleation and increase resistivity, showing that C is incorporated as a shallow acceptor. It was found that Si had little effect on the growth of such nanowires except at high concentrations, where growth along (*111*) decreased and growth along (*110*) increased; Si was observed to reduce resistivity, thus increasing carrier mobility. Chen *et al.* [30] found that incorporation of N in heterostructured InAs quantum dots led to an asymmetric line shape in the photoluminescence curve and a large series resistance. Schwartz *et al.* [31] found that p-doped (i.e., Zn) InAs(*110*) led to surface electrostatic effects. Zn atoms were found to attract holes, leading to variations in STM images. Additionally, Yonenaga [32] observed that Zn acceptors in InAs, increase the velocity of α dislocations and reduce that of β dislocations. Lin *et al.* [33], and Hoffman *et al.* [34], found that Be-doped InAs heterostructured superlattices (SL) go from *n*-type to *p*-type behavior and that dark currents can be minimized. Sankowska *et al.* [35], observed that Be doping in heterostructured SL altered the lattice parameter, inducing strains within the material that could alter the electronic structure.

An important experimental condition, not considered in the present simulations, is the presence of oxygen in the growth chamber. The oxygen can come from several sources. As an example, the adsorption energy of atomic O (where μ_O comes from the per atom DFT energy of O_2) adsorbing on the trench dimer of the InAs(*001*) $\alpha_2(2 \times 4)$ surface reconstruction, is found to be $\boldsymbol{E}_{\mathbf{ads}} = -1.60$ eV. Sulfurization of a material is often used to prevent oxygenation. Calculating the adsorption energy of S (where μ_S is the per atom DFT energy of a cluster model) on the $\alpha_2(2 \times 4)$ reconstruction, gives $E_{\mathbf{ads}} = -0.54$ eV.

Figure 14 shows the effects of O and S on the surface states of the As atom in the trench dimer of InAs(*001*) $\alpha_2(2 \times 4)$, previously shown in Figs. 5 and 6. Oxygen adsorption slightly increases surface states on the $\alpha_2(2 \times 4)$ reconstruction. Sulfur can reduce the defect states near the bandgap. But, a pronounced peak persists about 1.0 eV below $\boldsymbol{E}_{\boldsymbol{F}}$. Previous experimental work has shown that S has the opposite effect as the presence of Zn on electronic properties of InAs(*110*) [30], and that the presence of S donors reduces the speed of both α and β dislocations [31].

Going further down the oxygen group, Se could be a useful dopant, if it follows the trend of pushing the main peak further down into the valence bands. It may also lead to unique chemical-physical properties as it directly follows As in filling the *4p* subshell.

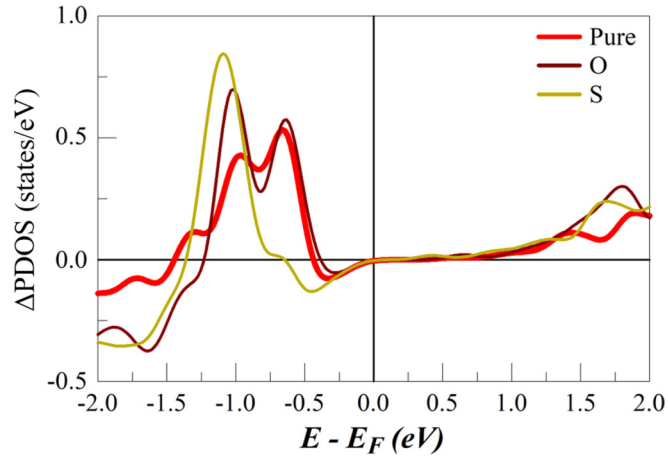

FIG. 14. Surface states on the clean, O-, and S-doped InAs(*001*) $\alpha_2(2 \times 4)$ surface reconstruction. Relative to the pure or O-doped surface, S doping pushes the main peak of the surface states deeper into the valence band.

V. CONCLUSIONS

Changes to the electronic structure from over half a dozen dopants deposited on half a dozen low-index surface reconstructions of InAs were studied. PDOS difference analysis was shown to be a useful tool in comparing such changes, so long as the proper background is subtracted, i.e., the PDOS of the bulk atoms. Aromaticity in local atomic structure was found to be a motivating influence, in particular for the group III element (indium) and the given dopant, for surface reconstruction and the elimination of surface states in pure and doped systems.

Biologic dopants (C,H,O,N) typically create more surface and gap states beyond those remaining from relaxation or reconstruction, rendering surface As atoms potentially more reactive and possibly leading to charge accumulation or depletion. Such elements typically cost energy to attach to low-index surfaces.

For certain surfaces, Si adsorption was able to reduce the number of electronic defect states. Zn and especially Be generally reduced surface states, in some instances nearly eliminating them. Be has a noted affinity to attach in any bonding motif to all the surfaces studied. Doping with Be or Zn pushed the surface states of As dimers deeper into the valence band by returning the As atoms to their unreconstructed positions. However, the surface states were not eliminated due to the adatom dopant leaving the As with one dangling bond. For the (*111*)B As trimer, these dopants nearly eliminate the surface states of the selected atom of the undoped surface. This is at the expense of opening the trimer, inducing different surface states. STM experiments should be carried out that search for the formation of zig-zag chains in Be- and Zn-doped (*111*)B surfaces.

For typical experimental conditions, O pollution could be a concern. However, S can be used to prevent oxygenation and can somewhat improve electronic properties over O-doped or pure InAs(*001*) $\alpha_2(2 \times 4)$. When the goal is to minimize surface states or similar defect states (e.g., GB interface states), experiments should strive to produce surfaces in the (*111*)A orientation, as its In-vacancy reconstruction is nearly planar at the surface interface and thus has minimal surface states. The (*110*) and (*112*)A (2×1) surfaces also show relatively small surface states. If the crystal orientation cannot be controlled, Be or Zn doping may offer promise.

While the above simulations doped with adatoms up to $\sim$0.1 ML coverage, which could be relevant to the field of solotronics, doping at higher concentrations may be beneficial in removing the surface state. Likewise, some dopants (whether by sintering or direct deposition) would be in the form of small molecules or clusters. These issues are left for future inquiries. Similarly, the effects from other metalloids and neighbors in the periodic table of In or As, as well as other light alkaline earth metals, should be investigated and is a topic for future research.

ACKNOWLEDGMENTS

This material is based upon work supported by the United States Air Force under Contract No. FA8650-16-C-7636. Any opinions, findings and conclusions or recommendations expressed in this material are those of the author(s) and do not necessarily reflect the views of the United States Air Force. This research was developed with funding from the Defense Advanced Research Projects Agency (DARPA). The views, opinions and/or findings expressed are those of the author and should not be interpreted as representing the official views or policies of the Department of Defense or the U.S. Government. We acknowledge financial support from the National Science Foundation through Grant No. DMS-1440415. We thank Minh Nguyen, Enrico Bellotti, Altynbek Murat, and Rajesh Rajavel for many crucial discussions. J.D. acknowledges helpful discussions with Lucy Gutierrez.

[1] J. Wei, J. M. Murray, J. Barnes, L. P. Gonzalez, and S. Guha, Determination of the temperature dependence of the band gap energy of semiconductors from transmission spectra, J. Electron. Mater. **41**, 2857 (2012).

[2] M. Mikhailova, N. Stoyanov, I. Andreev, B. Zhurtanov, S. Kizhaev, E. Kunitsyna, K. Salikhov, and Y. Yakovlev, Optoelectronic sensors on GaSb- and InAs-based heterostructures for ecological monitoring and medical diagnostics, Proc. SPIE **6585**, 658526 (2007).

[3] J. Wagner, J. Schmitz, F. Fuchs, U. Weimar, N. Herres, G. Tränkle, and P. Koidl, Structural characterization of InAs/(GaIn)Sb superlattices for IR optoelectronics, Mater. Res. Soc. Proc. **421**, 39 (1996).

[4] H. Yamaguchi and Y. Horikoshi, Surface structure transitions on InAs and GaAs (001) surfaces, Phys. Rev. B **51**, 9836 (1995).

[5] R. Magri and A. Zunger, Theory of optical properties of segregated InAs/GaSb superlattices, IEEE Proc. Optoelectronics **150**, 409 (2003).

[6] V. Blum, R. Gehrke, F. Hanke, P. Havu, V. Havu, X. Ren, K. Reuter, and M. Scheffler, *Ab initio* molecular simulations with numeric atom-centered orbitals, Comput. Phys. Commun. **180**, 2175 (2009).

[7] X. Ren, P. Rinke, V. Blum, J. Wieferink, A. Tkatchenko, A. Sanfilippo, K. Reuter, and M. Scheffler, Resolution-of-identity approach to Hartree-Fock, hybrid density functionals, RPA, MP2, and GW with numeric atom-centered orbital basis functions, New J. Phys. **14**, 053020 (2012).

[8] S. V. Levchenko, X. Ren, J. Wieferink, R. Johanni, P. Rinke, V. Blum, and M. Scheffler, Hybrid functionals for large periodic systems in an all-electron, numeric atom-centered basis framework, Comput. Phys. Commun. **192**, 60 (2015).

[9] A. Tkatchenko and M. Scheffler, Accurate Molecular Van Der Waals Interactions from Ground-State Electron Density and Free-Atom Reference Data, Phys. Rev. Lett. **102**, 073005 (2009).

[10] J. P. Perdew, K. Burke, and M. Ernzerhof, Generalized Gradient Approximation Made Simple, Phys. Rev. Lett. **77**, 3865 (1996).

[11] J. Heyd, G. E. Scuseria, and M. Ernzerhof, Hybrid functionals based on a screened Coulomb potential, J. Chem. Phys. **118**, 8207 (2003).

[12] J. Heyd, G. E. Scuseria, and M. Ernzerhof, Erratum: Hybrid functionals based on a screened Coulomb potential [J. Chem. Phys. 118, 8207(E) (2003)], J.Chem. Phys. **124**, 219906 (2006).
[13] O. A. Vydrov, J. Heyd, A. V. Krukau, and G. E. Scuseria, Importance of short-range versus long-range Hartree-Fock exchange for the performance of hybrid density functionals, J. Chem. Phys. **125**, 074106 (2006).
[14] P. M. Koenraad and M. E. Flatté, Single dopants in semiconductors, Nat. Mater. **10**, 91 (2011).
[15] J. Fernández Rossier, Quantum engineering, Nat. Mater. **12**, 480 (2013).
[16] J. Kobak, T. Smoleński, M. Goryca, M. Papaj, K. Gietka, A. Bogucki, M. Koperski, J.-G. Rousset, J. Suffczyński, and E. Janik *et al.*, Designing quantum dots for solotronics, Nat. Commun. **5**, 3191 (2014).
[17] A. Zangwill, *Physics at Surfaces* (Cambridge University Press, Cambridge, 1988).
[18] C. Ratsch, Strain-induced change of surface reconstructions for InAs(001), Phys. Rev. B **63**, 161306(R) (2001).
[19] C. Ratsch, W. Barvosa-Carter, F. Grosse, J. H. G. Owen, and J. J. Zinck, Surface reconstructions for InAs(001) studied with density-functional theory and STM, Phys. Rev. B **62**, R7719 (2000).
[20] J. L. A. Alves, J. Hebenstreit, and M. Scheffler, Calculated atomic structures and electronic properties of GaP, InP, GaAs, and InAs (110) surfaces, Phys. Rev. B **44**, 6188 (1991).
[21] E. Pehlke, N. Moll, A. Kley, and M. Scheffler, Shape and stability of quantum dots, Appl. Phys. A Mater. Sci. Process. **65**, 525 (1997).
[22] A. Taguchi and K. Kanisawa, Stable reconstruction and adsorbates of InAs(111)A surface, Appl. Surf. Sci. **252**, 5263 (2006).
[23] A. Taguchi, First-principles investigations of surface reconstructions of an InAs(111)B surface, J. Cryst. Growth **278**, 468 (2005).
[24] A. Höglund, C. W. M. Castleton, M. Göthelid, B. Johansson, and S. Mirbt, Point defects on the (110) surfaces of InP, InAs, and InSb: A comparison with bulk, Phys. Rev. B **74**, 075332 (2006).
[25] M. Nguyen (private communication, 2017).
[26] H. A. Craddock, *Oilfield Chemistry and its Environmental Impact* (Wiley, New York, 2018).
[27] R. Miotto, G. P. Srivastava, and A. C. Ferraz, Theoretical studies of the initial stages of Zn adsorption on GaAs(001-2 × 4), Phys. Rev. B **62**, 13623 (2000).
[28] C. W. M. Castleton, A. Höglund, M. Göthelid, M. C. Qian, and S. Mirbt, Hydrogen on III-V (110) surfaces: Charge accumulation and STM signatures, Phys. Rev. B **88**, 045319 (2013).
[29] H. Ghoneim, P. Mensch, H. Schmid, C. D. Bessire, R. Rhyner, A. Schenk, C. Rettner, S. Karg, K. E. Moselund, H. Riel, and M. T. Bjork, *In situ* doping of catalyst-free InAs nanowires, Nanotechnology **23**, 505708 (2012).
[30] J.-F. Chen, R.-S. Hsiao, Y.-C. Chen, Y.-P. Chen, M.-T. Hsieh, J.-S. Wang, and J.-Y. Chi, Effect of Nitrogen Incorporation into InAs layer in InAs/InGaAs self-assembled quantum dots, Jpn. J. Appl. Phys. **44**, 6395 (2005).
[31] A. Schwarz, W. Allers, U. D. Schwarz, and R. Wiesendanger, Detection of doping atom distributions and individual dopants in InAs(110) by dynamic-mode scanning force microscopy in ultrahigh vacuum, Phys. Rev. B **62**, 13617 (2000).
[32] I. Yonenaga, Dynamic behavior of dislocations in InAs: In comparison with III-V compounds and other semiconductors, J. Appl. Phys. **84**, 4209 (1998).
[33] Y. Lin, D. Wang, D. Donetsky, G. Belenky, H. Hier, W. L. Sarney, and S. P. Svensson, Minority carrier lifetime in beryllium-dopedu; inas/inassb strained layer superlattices, J. Electron. Mater. **43**, 3184 (2014).
[34] D. Hoffman, B.-M. Nguyen, P.-Y. Delaunay, A. Hood, M. Razeghi, and J. Pellegrino, Beryllium compensation doping of InAs/GaSb infrared superlattice photodiodes, Appl. Phys. Lett. **91**, 143507 (2007).
[35] I. Sankowska, A. Jasik, J. Kubacka-Traczyk, J. Z. Domagala, and K. Regiński, Role of beryllium doping in strain changes in II-type InAs/GaSb superlattice investigated by high resolution X-ray diffraction method, Appl. Phys. A **108**, 491 (2012).